A single layer deposition of Li-doped mesoporous TiO2 beads for low-cost and efficient dye-sensitized solar cells

Golvari, P.; Nouri, Esmaiel; Mohsenzadegan, N.; Mohammadi, M. R.; Martinez-Chapa, S. O.

A single layer deposition of Li-doped mesoporous TiO₂ beads for low-cost and efficient dye-sensitized solar cells

P. Golvari[a], E. Nouri[a], N. Mohsenzadegan[a], M.R. Mohammadi[*a,b] and S.O. Martinez-Chapa[c]

[a] *Department of Materials Science and Engineering, Sharif University of Technology, Azadi St., Tehran, Iran*

[b] *Tecnologico de Monterrey, Escuela de Ingeniería y Ciencias, Campus Puebla, Vía Atlixcáyotl 2301, Reserva Territorial Atlixcáyotl, CP 72453 Puebla, Pue, Mexico*

[c] *School of Engineering and Sciences, Tecnologico de Monterrey, Ave. Eugenio Garza Sada 2501, Monterrey 64849, NL, Mexico*

Abstract

Herein, we report a new strategy for improving the efficiency and reducing the fabrication cost of dye-sensitized solar cells (DSCs) by elimination of the three- or four-fold layer deposition of TiO₂. This is performed by replacing a single layer deposition of mesoporous TiO₂ beads, with sub-micrometer size, high surface area and tunable pore size, synthesized by a combination of sol-gel and solvothermal methods. Furthermore, superior electronic properties raised by a reduction in electronic trap states are achieved through doping of pristine TiO₂ beads with lithium. The beads show spherical shape with monodispersed texture consisting of anatase-TiO₂ nanocrystals and ultra-fine pores. The outstanding light scattering and harvesting characteristics of the beads are emerged from a combination of tailored morphology and crystal structure. These have resulted in 40% increase in a solar to electric power conversion efficiency, for a single spin-coated film without an additional scattering layer and pre- and post-treatment with TiCl₄ solution, compared to the reference nanoparticulate TiO₂ device.

Keywords: Dye-sensitized solar cell; single layer deposition; Li-doped TiO_2 beads; bandgap tuning.

1. Introduction

The urgency for development of clean electrical energy is appreciated today more than ever to reduce carbon dioxide gas emissions and global warming effect. Solar energy is considered as one of the most promising sources for the clean electrical energy, due mainly to its abundance and reliability. A solar cell is a photovoltaic device that converts the solar energy directly into electricity by the photovoltaic effect. Dye-sensitized solar cells (DSCs), proposed in 1991 by Gratzel and O'reagen[1], have been extensively studied due to their low fabrication cost, nontoxicity of the materials involved[2,3] and good potential in the form of flexible device[4,5] and improved stability.[67] The main component of a DSC is a photoanode electrode carrying a nanostructured oxide semiconductor, typically mesoporous TiO_2. Photogenerated electrons inject from dye-sensitizer into the conduction band of crystalline TiO_2 and then diffuse through the mesoporous network of photoanode. Light scattering of the incident light in DSC devices is a major challenge that has to be improved in terms of transport characteristics of charge carriers and light-harvesting. In the past few years, several approaches have been pursued by size and morphology engineering of TiO_2 semiconductor layer to improve light scattering of the photoanode.[8,9,10,11] In fact, incident light scattering can be achievable by large particles with diameters comparable to the wavelength of the incident light, i.e., submicron particles. Deposition of a single layer, composed of mixtures of nanoparticles and large particles, and double-layer, made of nanoparticulate under-layer as a light-absorber and a coarse top-layer as light scattering film, are two main approaches to encourage light scattering property of the photoanode electrode.[12] Among the most prominent approaches

taken over the years is the incorporation of a scattering layer in the form of double-layer electrode consisting of TiO_2 with various potentially scattering morphologies such as metal titanates,[13] hollow spheres,[14] dandelion-like,[15] nanocubes,[16] corn-like nanowires,[17] octahedron-like particles,[18] nanotubes[19] and spherical York-shell-like[20] structures. Although these approaches are proper configuration for efficient utilization of the solar spectrum, they have some limitations such as enhanced internal resistance and lowered accessible surface for dye loading. In addition, the preparation procedure of double-layer films is complex, since different TiO_2 precursors as well as different deposition techniques are required. An alternative approach to overcome these limitations has been to design hierarchical mesoporous TiO_2 structures.[21] The hierarchical structures not only have exceptionally high surface area due to abundance of mesopores, but also are capable of scattering light within the active layer due to their size resembling wavelength of the incident light. Therefore, it is possible to simplify and reduce fabrication cost of the device in such a way that solely a deposition of a single layer TiO_2 film would be sufficient to achieve a highly efficient photoactive layer. Mesoporous crystalline TiO_2 beads as promising features of the hierarchical structures have recently gained considerable attraction as photoanode of DSC devices.[22,23,24] The results showed that the mesoporous beads can enhance the light harvesting within the photoanode without sacrificing the available surface for dye loading, thereby increasing the photon-to-current conversion efficiency. There are several methods such as decreasing bandgap of TiO_2 by doping a foreign ion into the TiO_2 structure to enhance its electron injection.[25] The ion incorporates into the TiO_2 lattice, creating subsidiary Fermi level boosts this phenomenon. Further improvement of photovoltaic characteristics of TiO_2 beads by doping some impurities such as N_2[26] and Fe[27] into the semiconductor TiO_2 has been reported. Such enhancement is attributed either to passivation of electronic defect states[28] or enhanced electron trapping,[29] thereby lowering the recombination rate

of electron-hole pairs. It has been demonstrated that perovskite solar cells prepared using Li-doped TiO_2 electrodes produce substantially higher performances compared with undoped electrodes due to their superior electronic properties, by reducing electronic trap states enabling faster electron transport.[30] So far, no work has been reported on the performance of Li-doped mesoporous TiO_2 beads as light scattering sector in photoanode of DSC devices. Since Li^+ has a lower number of valence electrons than Ti^{4+}, the excess holes may create an acceptor band near TiO_2 valence band. The migration of electrons from valence to acceptor band could happen easier due to the lower bandgap between the valence and acceptor.

In the present work, we have focused on synthesis of Li-doped mesoporous TiO_2 beads with various atomic ratios by a two-step sol-gel and solvothermal procedure for solar cell applications. Our aim was to simplify the preparation of DSC by a single deposition of TiO_2 beads for a highly efficient photoanode electrode. The impact of Li introduction is studied on phase composition, morphology, optical properties, incident light scattering and photovoltaic performance of fabricated DSC devices.

2. Experimental section

2.1. Synthesis of mesoporous TiO₂ beads

Mesoporous anatase-TiO_2 beads with diameter of 120-1900 nm were synthesized according to a two-step procedure previously reported by Chen et al.[31] In the first step, 0.5 g of hexadecylamine (HDA) with a purity of 98% (Aldrich), as a structure-directing agent, was dissolved in 25 mL ethanol, followed by addition of 0.27 mL deionised water and 0.2 mL of aqueous KCl (with a purity of 99.5%, Merck) solution (0.1 M). KCl controls the monodispersity of the sol-gel derived powders by adjusting the ionic strength of the solution. In a separate beaker,

1.15 mL of titanium tetraisopropoxide (TTIP) with a purity of 97% (Aldrich) were dissolved in 25 mL ethanol and immediately added to the prior solution under vigorous stirring. A milky suspension was instantly formed as a result of hydrolysis and condensation reactions of the sol-gel process. It was found that the reaction time was decreased with increasing water content. The white suspension was kept in the atmosphere for 18 h to deposit all sediments, separated with decanting, washed with ethanol and finally dried at room temperature. The diameter of beads was tailored by controlling the Ti:H_2O molar ratio. This was carried out by further addition of 0.20, 0.27, 0.33, 0.40, 0.46 and 1.60 mL deionised water into the first solution, as listed in **Table 1**.

Table 1. The impact of Ti: H_2O molar ratio on diameter of synthesized TiO_2 beads by the sol-gel process, measured by SEM images in **Figure 1**.

Structure	Sample	Ti:H_2O molar ratio	Li:Ti molar ratio	Bead diameter (nm)
Pristine TiO_2 beads	B6	1:6	0	1700 ± 80
	B7	1:7		900 ± 60
	B8	1:8		350 ± 40
	B9	1:9		300 ± 40
	B10	1:10		300 ± 40
	B27	1:27		200 ± 20
	B27NK	1:27		200 ± 60
Li-doped TiO_2 beads	B7L5	1:7	0.0005:1	1000 ± 80
	B7L20	1:7	0.002:1	1000 ± 80

For sample B27NK, no KCl solution was added in the first solution, just contained 0.20 mL deionized water. In the second step, the sol-gel derived powders were treated solvothermally to obtain the mesoporous TiO_2 beads. 0.4 g of the powder was dispersed in a mixture of 18 mL ethanol and 9 mL deionised water and heated in a Teflon-lined stainless-steel autoclave for 16 h at 160 °C, and subsequently cooled naturally to room temperature. The collected precipitates (i.e.,

mesoporous beads) were washed with ethanol, dried at room temperature and finally annealed at 500 °C for 2 h.

2.2. Li-doped mesoporous TiO$_2$ beads

Lithium was doped into mesoporous TiO$_2$ beads via in-situ exposing of samples to LiCO$_3$ solution in the sol-gel process (i.e., the first step), while the above mentioned deionised water was partially replaced by different amounts of aqueous LiCO$_3$ solution (0.05 M), maintaining Ti:H$_2$O ratio = 1:7. Therefore, B7 sample was used as the reference (i.e., undoped TiO$_2$ beads) and B7L5 and B7L20 were prepared by addition of 0.02 mL and 0.08 mL of the aqueous LiCO$_3$ solution corresponding to Li:Ti molar ratio of 0.0005:1 and 0.002:1, respectively (See **Table 1**).

2.3. Synthesis of TiO$_2$ nanoparticles

TiO$_2$ nanoparticles were also synthesized by a combination of sol–gel and hydrothermal methods based on our previous work,[32] to provide an additional control sample. The performance of cells made of mesoporous beads were compared with that composed of anatase-TiO$_2$ nanoparticles. Briefly, TTIP was dissolved in 1-octanol with a purity of 99% (Merck) to form a 0.55 M precursor solution. Deionised water was added into the above solution, with a molar ratio of H$_2$O:Ti = 3.3:1, to form the TiO$_2$ sol. The sol was hydrothermally treated in a Teflon-lined stainless-steel autoclave at 180 °C for 4 h. The final products (i.e., TiO$_2$ nanoparticles, NP) were washed with ethanol and deionised water and dried at room temperature.

2.4. Preparation of photoanode electrodes

6

TiO$_2$ pastes with excellent stability and rheology were prepared using the synthesized pristine and Li-doped TiO$_2$ beads according to our previously reported procedure.[33] The pastes were spin-coated on cleaned fluorine-doped tin oxide (FTO) substrates in two consecutive steps with coating speeds of 3500 rpm and 4500 rpm each for 15 sec, followed by annealing at 400 °C for 2 h. Our telic photoanodes were obtained by soaking the electrodes in a 0.5 mM ethanol solution of N719 dye (Ruthenium 535-bisTBA; Solaronix, Aubonne, Switzerland) for 18 h, followed by washing unloaded dyes by ethanol. It should be noted that the photoanode electrode was prepared by a single deposition of pristine and Li-doped TiO$_2$ beads with neither pre- and post-treatment with TiCl$_4$ solution, nor the anti-reflecting layer and the light scattering layer.

2.5. DSC assembly

The counter electrode was made by drop-coating of H$_2$PtCl$_6$ solution (2 mg Pt in 1 mL ethanol) on clean FTO substrate, carrying a small hole to allow the introduction of the liquid electrolyte using vacuum. The wet electrode was dried and then heat-treated at 400 °C for 30 min. The dye-soaked photoanode and Pt-coated counter electrode were sandwiched using a thin thermoplastic frame (Surlyn, Solaronix) that melted at 125 °C. DSC devices were fabricated by vacuum injecting of a redox iodine-based electrolyte consisting of 0.5 mol/L 1-butyl-3-methylimidazolium iodide, 0.1 mol/L lithium iodide, 0.05 mol/L iodine and 0.5 mol/L tert-butylpyridine in acetonitrile.

2.6. Characterisation and measurements

The crystal structure of pristine and Li-doped TiO$_2$ beads was characterized by X-ray diffraction (XRD) using a X'pert Pro MPD diffractometer (PANalytical, Kassel-Waldau,

Germany), operating at 30 kV, 10 mA at 2θ of 20−80° (Cu Kα, λ = 1.5406 Å). The FT-IR spectra of samples were recorded by a spectrometer (SHIMADZU-IRsolution, 8400S series, Japan) in the wavenumber range between 400 and 4000 cm^{-1}. The microstructural graphs were imaged by a field emission scanning electron microscope (FE-SEM), Mira-3 microscope (TESCAN, Kohoutovice, Czech Republic). The specific surface area and pore size distribution of synthesized beads were determined using a Micromeritics TriStar 3000 analyzer (Micromeritics, Aachen, Germany) by Brunauer-Emmett-Teller (BET) and Barret-Joyner-Halenda (BJH) equations at 77.35 K. Diffuse reflectance spectroscopy (DRS) of pristine and Li-doped TiO_2 beads and their corresponding optical bandgap were estimated using a UV–visible spectrometer, AVASPEC-2048-TEC, Netherland, carrying a $BaSO_4$ disc as a reflectance standard. The amount adsorbed N719-dye molecules on photoanodes was spectroscopically determined by a UV-vis spectrophotometer (6705 JENWAY, Staffordshire, UK) in a forced dye desorption into an aqueous solution of 0.1 molar NaOH. The photoelectrical metrics of DSC devices were investigated using a Zahner CIMPA-pcs solar simulator (Zahner, Kronach, Germany) under standard test conditions at one Sun (irradiance of 100 mW/cm^2, AM 1.5) with a scan rate of 50 mV/s. It should be noted that each batch included five devices and the average values were reported.

3. Results and discussion

Figure 1 illustrates the impact of $Ti:H_2O$ molar ratio on microstructure of prepared mesoporous TiO_2 beads by a combination of sol-gel and solvothermal methods. The spherical beads, composed of fine nanocrystals, had tunable overall dimeter ranging from 100 nm to 2 μm, as presented in **Table 1**. An intense reduction in diameter of the beads, from 1700 ± 80 nm to 350 ± 40 nm, was achieved by decreasing $Ti:H_2O$ ratio down to 1:8 (**Figures 1 (a-c)**), followed by

slightly reduction down to 200 ± 20 nm with further decrease in Ti:H_2O ratio to 1:27 (**Figures 1 (d-f)**). B7 would be an ideal candidate for light scattering in photoanode of the cell since it showed monodisperse beads with a diameter around 900 nm (i.e., comparative particle size to the optical wavelengths). The particle size distribution became more polydisperse (200 ± 60 nm) and more dimers were found when the synthesis process is conducted without KCl solution **(Figure 1g).**
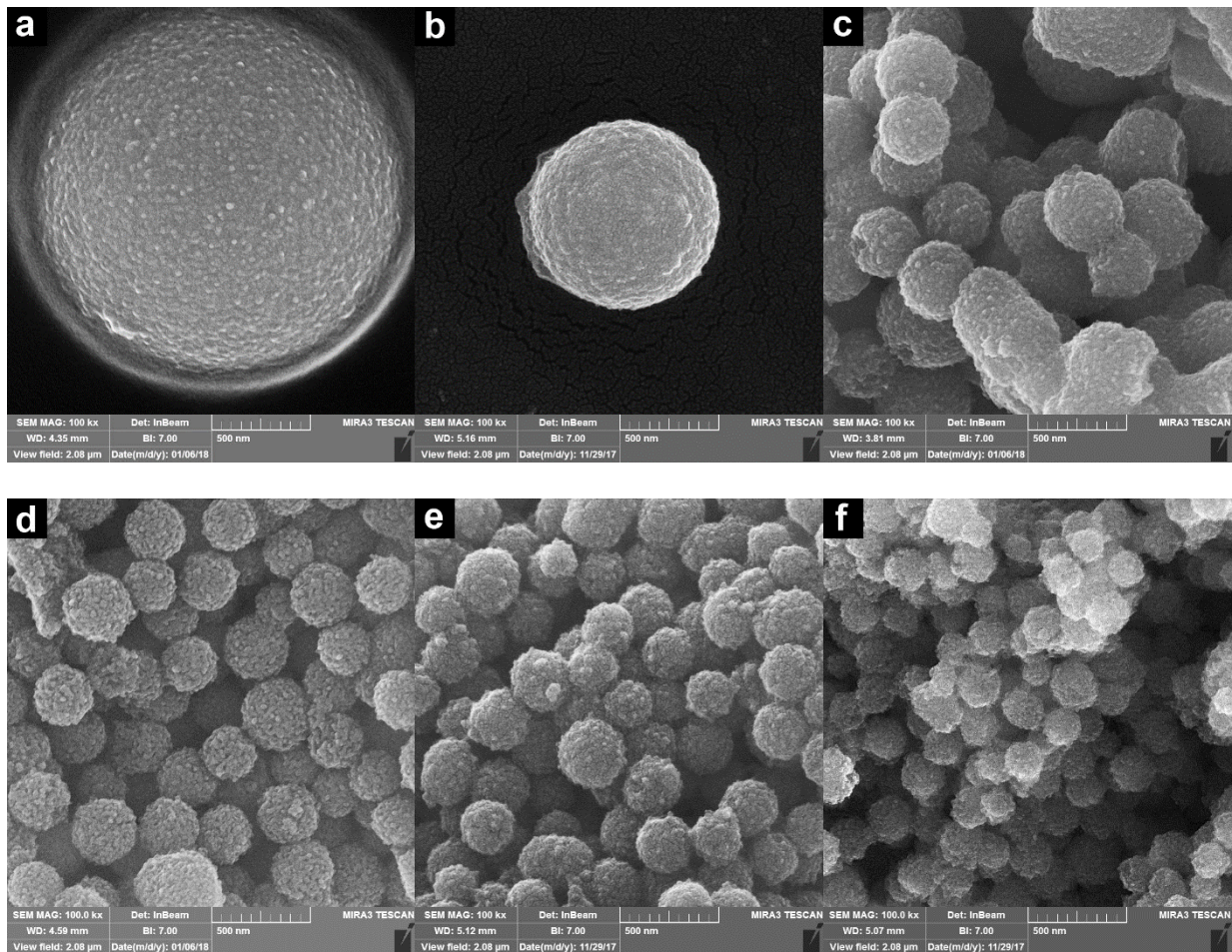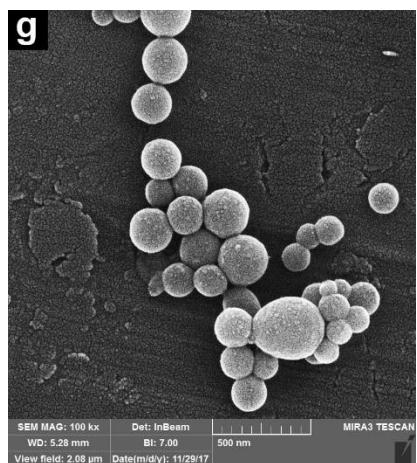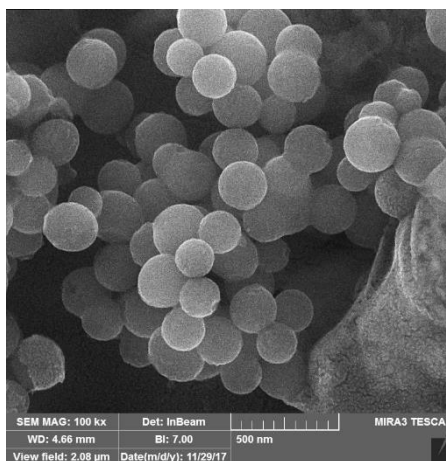
Figure 1. FESEM images of synthesized mesoporous TiO_2 beads by a combination of sol-gel and solvothermal methods with various $Ti:H_2O$ molar ratios: (a) B6, (b) B7, (c) B8, (d) B9, (e) B10 (f) B27 and (g) B27NK.

The beads with large particle size give the film the ability to scatter light. To realize high-efficiency DSCs, a double layer film containing a scattering layer made of 400 nm particles is coated on top of an active layer composed of the nanocrystalline TiO_2 layer. However, such configuration makes the fabrication process more complex and potentially increases the cost of manufacture. Moreover, the mesoporous beads provide sufficient surface area (see Figure 5) for dye loading, resulting in enhanced light harvesting.

The influence of solvothermal treatment on microstructure of TiO_2 beads is shown in **Figure 2**. It is evident that the spherical TiO_2 beads synthesized by sol-gel route had a smooth surface without obvious granular features (**Figure 2**), while their surfaces were roughly textured, composed of nanoparticles, with around 20% shrinkage in the diameter by subsequent solvothermal treatment. Therefore, a combination of sol-gel and solvothermal processes afforded individual, monodisperse beads with rough surfaces and high surface area.

Figure 2. FESEM image of synthesized TiO_2 beads by a sol-gel process (i.e., prior solvothermal treatment) with $Ti:H_2O$ molar ratio of 1:27.

Figure 3 shows the XRD patterns of synthesized pristine and Li-doped mesoporous TiO_2 beads. As illustrated in the inset of **Figure 3**, the main anatase peak of (1 0 1) plane was detected at $2\theta = 25.44°$ and $25.39°$ for the pristine (B7) and Li-doped (B7L5) TiO_2 beads, respectively. Both pristine and Li-doped beads highly conform to full-anatase pattern, indicating no changes in the crystal structure upon addition of Li ion. Since the Li^+ radius is greater than that of Ti^{4+} (0.76 nm vs. 0.60 nm), the substitution may induce the lattice expansion, resulting in a shift of anatase peak to the lower angles. Although for the replacement of Ti^{4+} by Li^+ ions some Ti–O bonds are broken, which leads to the formation of oxygen vacancies, the contraction of lattice caused by oxygen deficiency is eliminated through lattice expansion induced by the entrance of slightly larger lithium ions. The average crystallite size of both pristine and Li-doped TiO_2 beads was calculated to be around 11 nm, using Scherrer equation.
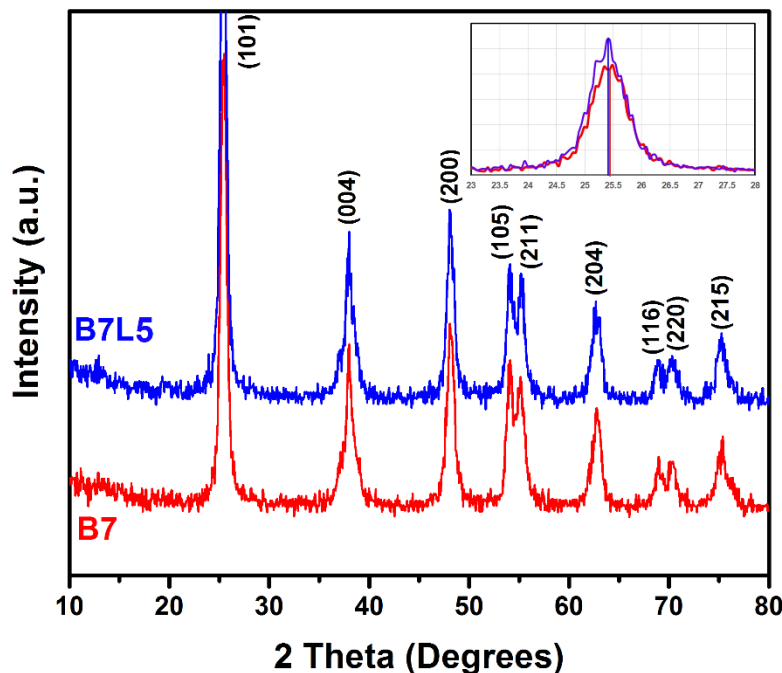
Figure 3. XRD patterns of pristine (B7) and Li-doped (B7L5) mesoporous TiO_2 beads.

The structural evolution of TiO_2 beads in the presence of lithium cations was studied by FT-IR spectroscopy and the results are shown in **Figure 4**. The FT-IR spectra of both pristine and Li-doped mesoporous TiO_2 beads show same bands at wavenumbers higher than 1000 cm^{-1}. The bands observed at 3414 and 2973 cm^{-1} are assigned to the vibrations of the hydroxyl group (O–H). The band located around 1633 cm^{-1} is attributed to bending modes of Ti–OH, due to atomic absorbed water. Two sets of peaks at 1383 cm^{-1} and 658 cm^{-1} are related to bending and stretching vibrations modes of Ti–O bands, respectively.[34] FTIR spectrum of Li-doped beads shows a significant shoulder-type peak at 498 cm^{-1}, which can be assigned to Li–O symmetrical stretching vibrations.[29] This further confirms the presence of lithium cations in the crystalline network of mesoporous TiO_2 beads.
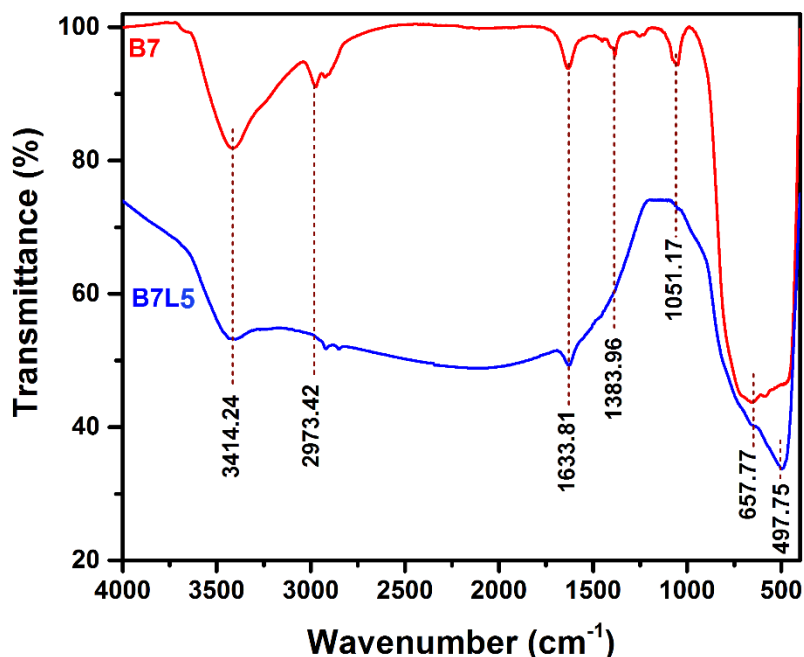
Figure 4. FT-IR spectra for pristine (B7) and Li-doped (B7L5) mesoporous TiO$_2$ beads.

BET isotherms obtained from N$_2$ gas adsorption–desorption into pristine and Li-doped mesoporous TiO$_2$ beads and the corresponding pore size distribution curves are shown in **Figure 5**. The resulted type IV isotherms prove that when relative pressures are too low, only monolayer formation is occurring and as the relative pressures increases higher than 0.5, N$_2$ gas condenses in the tiny capillary pores of the porous beads up to saturation pressure. The Li-doped beads exhibited a greater adsorbed N$_2$ volume before saturation, associated with a slightly higher S$_{BET}$ of 78.1 m^2/g, in comparison to 75.4 m^2/g for pure TiO$_2$ beads. In addition, the inset of **Figure 5** shows a similar pore size distribution curve for both beads, although the maximum peak was appeared at a smaller pore size for lithium containing sample. Such a porous characteristic of Li-doped beads promotes a more perfect skeletal medium for adsorption of dye molecules.
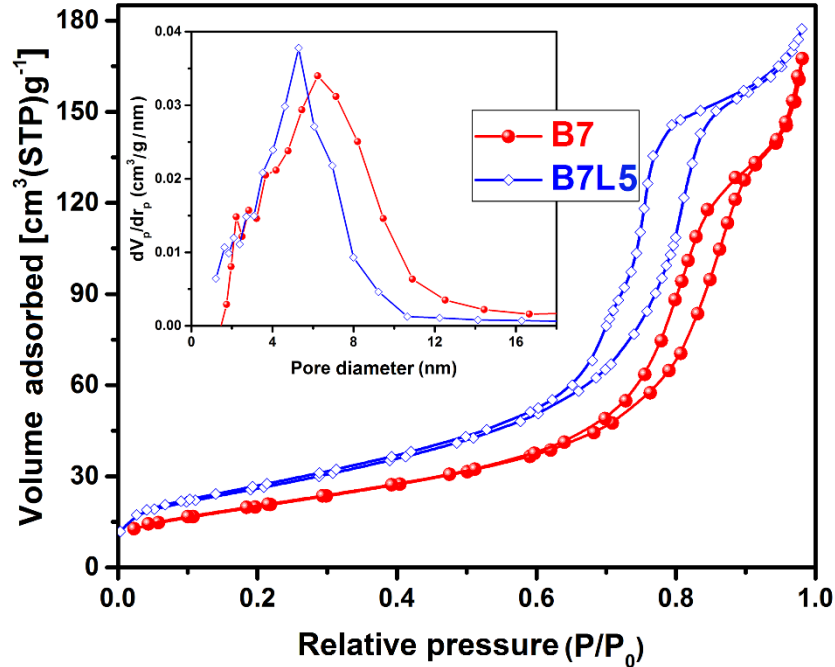
Figure 5. Nitrogen adsorption-desorption isotherm of pristine (B7) and Li-doped (B7L5) TiO$_2$ beads. The insets show pore size distribution curves.

As a comparison, the diffuse reflection spectra (DRS) and corresponding optical bandgap energy of pure and Li-doped mesoporous TiO$_2$ beads were measured (**Figure 6**). Both beads presented high diffuse reflection capabilities in the wavelengths higher than 400 nm. Such a high DRS property in the visible and near infrared regions indicates that the incident light would be efficiently scattered within the photoanode made up of mesoporous TiO$_2$ beads due to their comparable size to the wavelength of visible light.[13] It is noteworthy that Li-doped mesoporous TiO$_2$ beads exhibit a slightly higher light scattering property than pristine TiO$_2$ beads. This can be related to the lattice expansion, due to greater ionic radius of Li compared to that of Ti, and an increase in surface area inducing rougher surface by introduction of Li$^+$ into the TiO$_2$ lattice. The higher diffuse reflectance properties of Li-doped mesoporous TiO$_2$ beads under visible light irradiation is expected to improve the utilization of the solar spectrum in the DSCs.

14

Figure 6b exhibits the optical bandgap energy variation of TiO_2 beads in the presence of lithium cations, which determined based on Tauc model via extrapolating linear region of the plots of transformed Kubleka–Munk function versus the excited photon energy. It is evident that the bandgap energy of beads decreases remarkably with the introduction of Li ions into the TiO_2 lattice, being 3.19 eV and 2.06 eV for pristine and Li-doped mesoporous TiO_2, respectively. This verifies successful doping levels of lithium in the crystalline TiO_2 matrix without formation of undesired compounds. Therefore, the replacement of Ti^{4+} by Li^+ ions can effectively create a series of deep traps in the conduction band of TiO_2, which causes its downward shift.
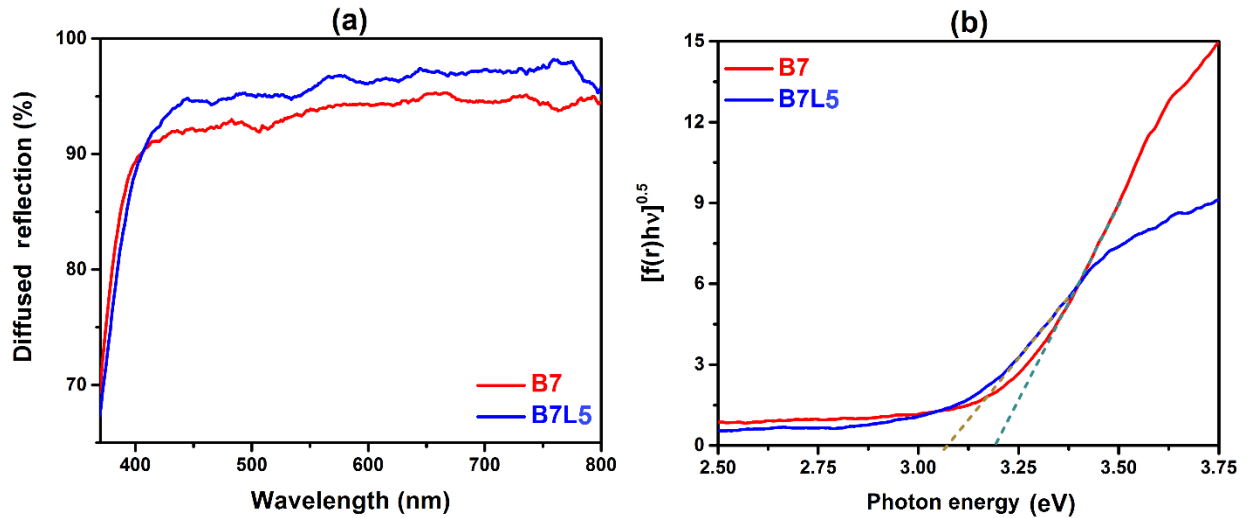
Figure 6. (a) Diffuse reflectance spectra and (b) relationship between the transformed Kubelka-Munk function versus exciting light energy along with extrapolated linear region for optical bandgap estimation of pristine (B7) and Li-doped (B7L5) mesoporous TiO_2 beads.

In addition, the substitution of Li^+ with three valence state less than that of the Ti^{4+} host atom, results in the formation of positively charged oxygen vacancy, which can act as an acceptor and decrease the donor density. The amount of the adsorbed dye greatly influences the short-circuit current and power conversion efficiency of the cells. Therefore, the impact of Li-doping on N719-

dye adsorption of the photoanodes made up of mesoporous TiO_2 beads is studied by UV-vis absorption spectra, as illustrated in **Figure 7**. TiO_2 photoanodes were first stored in a N719-dye solution for 18 h and then immersed in a NaOH solution (0.1 molar in water) to forcedly dye desorption. Matter-of-course all dye-loaded films had the same thickness of about 21 μm and almost equal macroscopic geometric area. The UV-vis absorption spectra of dye colored solutions showed five bands at 229, 244 and 307 nm wavelengths (UV region) along with the wavelengths of 371 and 496 nm (visible region). The UV region peaks are assigned to the ligand-centered charge-transfer transitions, whereas the visible region peaks are attributed to the metal-to-ligand charge-transfer transitions.[35]
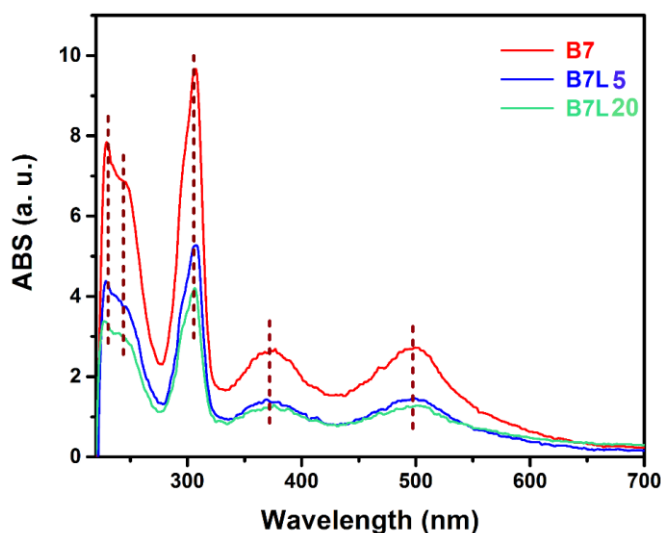
Figure 7. UV–Vis spectra of adsorbed N719-dye molecules from photoanodes made of single layer pristine and Li-doped mesoporous TiO_2 beads by using 0.1 M NaOH aqueous solution.

We can observe a lower dye loading on the photoanode when lithium ions are introduced, which can be explained by two facts. First, this phenomenon can be attributed to different interactions of Ti^{4+} and Li^+ with N719–dye molecules, raised by their different bond strengths. Considering the bonding energy of Ti-O (i.e., 666.5 ± 5.6 kJ/mol), which is almost two times greater than that of Li-O (i.e., 340.5 ± 6.3 kJ/mol), dye absorption capability of Li-doped TiO_2

beads would be less than that of pristine TiO_2 beads. Second, the adsorption of the dye molecules by the chemisorption on the thermodynamically stable Ti^{4+} sites is greater than that on Ti^{3+} surface defects produced by the doping process. It is also observed that higher level doping of Li into TiO_2 matrix leads to further decrease in dye absorption due to the above-mentioned facts.

The surface morphology and cross-sectional image of the photoanode composed of mesoporous TiO_2 beads is shown in **Figure 8**. Keeping in mind microstructure and morphology of synthesized beads (**Figure 1**), it is evident that the preparation process and heat treatment of photoanode using a homemade paste had no influence on morphology and average size of TiO_2 beads. The electrode showed uniform, homogeneous and porous structure as a result of removal of the additives. For a high efficiency DSC photoanodes needs to have high surface area with optimum porosity. The photoanode with thickness around 21 µm contained submicrometer-sized beads.

In order to improve the photovoltaic performance of the solar cells, the electron transport mechanism by reducing electronic trap states through Li doping has been reported.[30] We present the impact of this mechanism on the photocurrent density–potential (J–V) characteristics of the DSC devices made of Li-doped mesoporous TiO_2 beads, as shown in **Figure 9**. In addition, the corresponding photovoltaic parameters such as short-circuit current (Jsc), open-circuit potential (Voc), fill factor (FF) and power conversion efficiency (PCE) are summarized in Table 2.
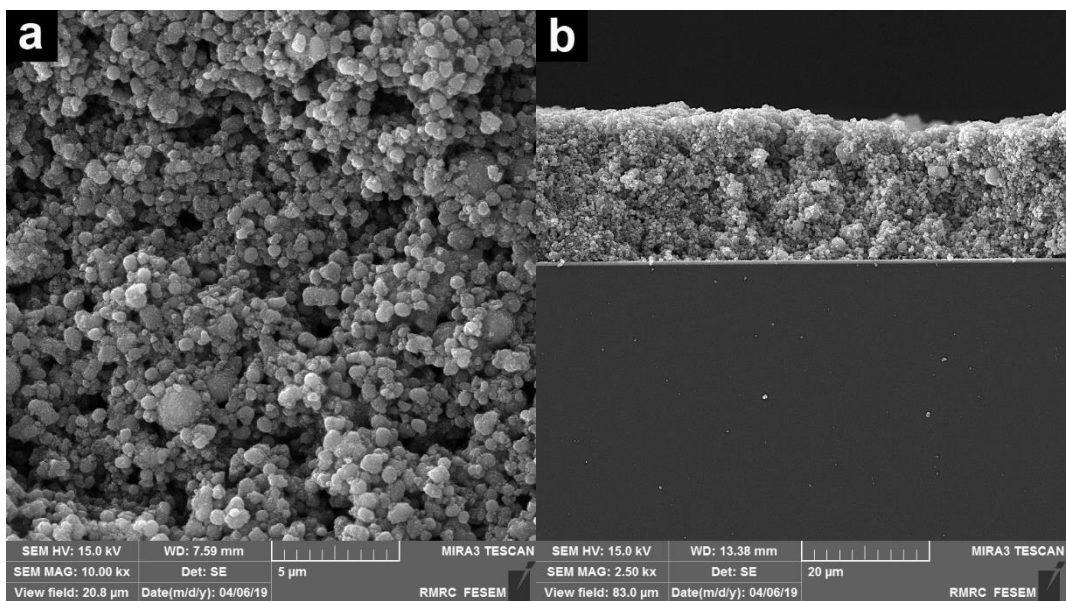
Figure 8. FE-SEM images of the photoanode made of mesoporous TiO_2 beads: (a) surface morphology and (b) cross-sectional view.

We found that DSCs based on mesoporous beads show higher Jsc and lower Voc than that made of nanoparticles. Moreover, the same trend in Jsc and Voc is observed with Li introduction and an increase in its concentration. As the difference between the Fermi level of the TiO_2 film and the electrolyte redox potential defines the maximum potential generated,[36] such reduction in Voc can be explained by a positive shift of the flat band potential by means of utilising beads and Li doping, resulting in lowering the Fermi level and conduction band of the pristine and doped beads. This phenomenon is consistent with the results obtained from DRS analysis, which shows a lower bandgap energy for Li-doped mesoporous TiO_2 beads (as shown in **Figure 6b**). It is well-known that the J_{SC} produced in a DSC device is essentially determined by the amount of sensitizer adsorbing which controls sunlight harvesting from solar illumination.[37] Although Li-doped photoanode exhibited lower dye-loading (shown in **Figure 7**) than the pristine beads, the resulting J_{SC} of Li-doped electrode is controlled by its electronic characteristics by creating deep traps in the

conduction band of TiO_2, leading to an increase in fraction of charge carriers (i.e., increasing the conductivity), and eventually enhancement in J_{SC}. Furthermore, replacing Ti^{4+} by Li^+ creates a series of deep traps, which causes the downward shift of conduction band. This can increase the offset of the conduction band and the lowest unoccupied molecular (LUMO) level, leading to an enhanced driving force for electron injection to the conduction band and increased the photocurrent density. Consequently, the enhancement in J_{SC} of DSC devices based on mesoporous TiO_2 beads can be explained by porosity and scattering modifications for the pristine beads and electron transport improvement through reducing electronic trap states for the Li-doped beads.
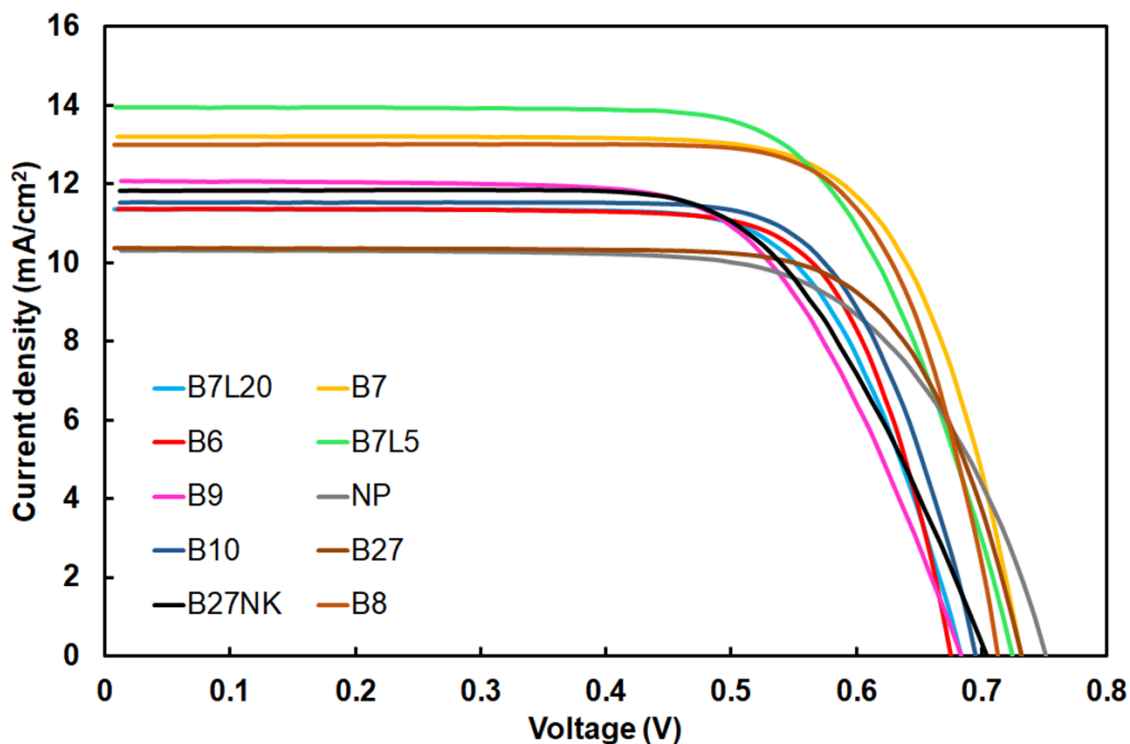
Figure 9. Impact of Li doping on the photocurrent density–potential curves of DSCs made of a single layer deposition of mesoporous TiO_2 beads, compared with the reference device based on TiO_2 nanoparticulate film.

Among all fabricated cells, B7L5 DSC (containing 0.0005 at.% Li) showed the highest PCE of 7.48%, being one of the highest efficiencies reported in the literature for DSCs based on a single layer deposition of TiO_2 without pre- and post-treatment with $TiCl_4$ solution using a redox iodine-based electrolyte and N719 dye. In addition, all fabricated devices showed good reproducibility due to low experimental error of the photovoltaic parameters. PCE of Li-doped TiO_2 based cell decreased with an increment in the dopant concentration up to 0.002 at.% raised by a drop in V_{OC}, as discussed earlier.

Table 2. Photovoltaic characteristics of fabricated DSCs by a single layer deposition of pristine and Li-doped mesoporous TiO_2 beads compared to that made of TiO_2 nanoparticles.

DSC	Photoanode	J_{SC} (mA/cm²)	V_{OC} (V)	FF	PCE (%)
NP	TiO_2 nanoparticles	10.30 ± 0.03	0.751 ± 0.02	0.686 ± 0.01	5.31 ± 0.236
B6		13.47 ± 0.02	0.676 ± 0.01	0.676 ± 0.01	6.79 ± 0.192
B7		13.15 ± 0.02	0.732 ± 0.01	0.734 ± 0.02	7.07 ± 0.302
B8	Pristine mesoporous TiO_2 beads	13.01 ± 0.03	0.713 ± 0.02	0.753 ± 0.01	6.98 ± 0.308
B9		13.23 ± 0.02	0.684 ± 0.02	0.661 ± 0.01	5.98 ± 0.277
B10		11.53 ± 0.03	0.695 ± 0.01	0.734 ± 0.02	5.88 ± 0.263
B27		10.37 ± 0.02	0.732 ± 0.01	0.737 ± 0.01	5.59 ± 0.164
B27NK		11.84 ± 0.03	0.704 ± 0.02	0.661 ± 0.02	5.51 ± 0.342
B7L5	Li-doped TiO_2 beads	14.82 ± 0.03	0.725 ± 0.01	0.696 ± 0.01	7.48 ± 0.227
B7L20		14.10 ± 0.03	0.683 ± 0.01	0.720 ± 0.01	6.93 ± 0.214

4. Conclusions

To summarize, we demonstrated cost-effective DSC with high efficiency raised by two approaches. In the first approach, the photoanode electrode was simplified by a single spin-coated titania film composed of mesoporous beads without an additional scattering layer and pre- and post-treatment with $TiCl_4$ solution. The diffuse reflectance of the beads was enhanced across the

500-800 nm wavelengths by tuning the size of the beads, their pores and their interconnections, resulted in a substantial enhancement in efficiency up to 7.07% when compared to the control device based on nanoparticulate titania film with PCE of 5.31%. Such enhancement was related to higher photocurrent and the improved charge collection efficiency in the spherical bead photoanodes. Our next approach was to improve the electron transport of the mesoporous TiO_2 beads aided by substitutional lithium dopant. Li doping of TiO_2 can enable faster electron injection and transport in the device by lowering the conduction band edge of TiO_2, reducing the concentration of sub-bandgap states and inducing a partial reduction of Ti^{4+} to Ti^{3+}. We showed that a DSC prepared on Li-doped mesoporous TiO_2 beads with optimum Li concentration of 0.0005 at.% achieved substantially higher performance of 7.48%, compared with the device based on pristine beads.

References

1 B. O'Regan and M. Grätzel, *Nature,* 1991, **353**, 737–740.

2 S. Galliano, F. Bella, M. Bonomo, G. Viscardi, C. Gerbaldi, G. Boschloo and C. Barolo, *Nanomaterials,* 2020, **10**, 1585.

3 F. Bella, L. Porcarelli, D. Mantione, C. Gerbaldi, C. Barolo, M. Grätzel and D. Mecerreyes, *Chem. Sci.*, 2020, **11**, 1485-1493.

4 F. Bella, A. Lamberti, A. Sacco, S. Bianco, A. Chiodonj and R. Bongiovanni, *J. Membrane Science*, 2014, **470**, 125-131.

5 F. Bella, A. Lamberti, S. Bianco, E. Tresso and C. Gerbaldi, *Adv. Mater. Technol.,* 2016, **1**, 1600002.

6 M. Imperiyka, A. Ahmad, S.A. Hanifah and F. Bella, *Physica B: Condensed Matter*, 2014, **450**, 151-154.

7 L. P. Teo, M. H. Buraidah and A. K. Arof, *Ionics,* 2020**, 26**, 4215–4238.

8 S. Hore, C. Vetter, R. Kern, H. Smit and A. Hinsch, *Energy Mater. Sol. Cells,* 2006, **90**, 1176–1188.

9 Y. C. Park, Y. J. Chang, B. G. Kum, E. H. Kong, J. Y. Son, Y. S. Kwon, T. Park and H. M. Jang, *J. Mater. Chem.,* 2011, **21**, 9582–9586.

10 Z. Andaji Garmaroudi, M. Abdi-Jalebi, M. R. Mohammadi and R. H. Friend, *RSC Advances*, 2016, **6**, 70895-70901.

11 K. Susmitha, M. Naresh Kumar, M. Gurulakshmi, L. Giribabu and M. Raghavender, *Sustainable Energy Fuels*, 2017, **1**, 439-443.

12 F. Bella, R. Bongiovanni, R. Senthil Kumar, M. Anbu Kulandainathan and A. Manuel Stephan, *J. Mater Chem. A*, 2013, **1**, 9033-9036.

13 S. Yang, H. Kou, J. Wang, H. Xue and H. Han, *J. Phys. Chem. C,* 2010, **114**, 4245-4249.

14 Y. Tabari-Saadi and M.R. Mohammadi, *J. Mater. Sci.: Mater. Electron.*, 2015, **26**, 8863-8876.

15 P. M. Gharavi and M. R. Mohammadi, *Solar Energy Materials and Solar Cells,* 2015, **137**, 113–123.

16 N. Sarvari and M.R. Mohammadi, *J. Am. Ceram. Soc.*, 2018, **101**, 293-306.

17 A. M. Bakhshayesh, M. R. Mohammadi, H. Dadar and D. J. Fray, *Electrochimica Acta,* 2013, **90**, 302–308.

18 Jia-Wei Shiu, Chi-Ming Lan, Yu-Cheng Chang, Hui-Ping Wu, Wei-Kai Huang and Eric Wei-Guang Diau, *ACS Nano,* 2012, **6**, 10862-10873.

19 H. Mokarami Ghartavol, M.R. Mohammadi, A. Afshar, F. Chau-Nan Hong and Yeau-Ren Jeng, *RSC advances*, 2016, **6**, 101737–101744.

20 K. Guo, M. Li, X. Fang, L. Bai, M. Luoshan, F. Zhang and X. Zhao*, J. Power Sources,* 2014, **264**, 35–41.

21 Y. Ding, T. Zhang, C. Liu, Y. Yang, J. Pan, J. Yao, L. Hu and S. Dai, *Sustainable Energy Fuels*, 2017, **1**, 520-528.

22 F. Sauvage, D. Chen, P. Comte, F. Huang, L. P. Heiniger, Y.B. Cheng, R.A. Caruso and M. Graetzel, *ACS Nano*, 2010, *4*, 4420–4425.

23 Y. Chen, F. Huang, W. Xiang, D. Chen, L. Cao, L. Spiccia, R. A. Caruso and Y. B. Cheng, *Nanoscale*, 2014, **6**, 13787-13794.

24 F. Huang, D. Chen, Y. Chen, R. A. Caruso and Y. B. Cheng, *J. Mater. Chem. C*, 2014, **2**, 1284-1289.

25 V. Prabhagar. M., M. Praveen Kumar, C. Takahashi, S. Kundu, T. N. Narayanan and D. K. Pattanayak, *New J. Chem.*, 2019, **43**, 14313-14319.

26 Jasmin S. Shaikh, Navajsharif S. Shaikh, Sawanta S. Mali, Jyoti V. Patil, Krishna K. Pawar, Pongsakorn Kanjanaboos, Chang Kook Hong, J. H. Kim and Pramod S. Patil, *Nanoscale*, 2018, **10**, 4987-5034.

27 W. Zhao, W. Fu, H. Yang, C. Tian, M. Li, J. Ding, W. Zhang, X. Zhou, H. Zhao and Y. Li, *Nano-micro letters*, 2011, **3**, 20–24.

28 V. Sivaram, E. J. W. Crossland, T. Leijtens, N. K. Noel, J. Alexander-Webber, P. Docampo and H. J. Snaith, *J. Phys. Chem. C,* 2014, **118**, 1821-1827.

29 T. N. Ravishankar, G. Nagaraju and J. Dupont, *Materials Research Bulletin,* 2016, **78**, 103–111.

30 F. Giordano, A. Abate, J. P. Correa Baena, M. Saliba, T. Matsui, S. H. Im, Shaik M. Zakeeruddin, M. K. Nazeeruddin, A. Hagfeldt and M. Graetzel, *Nature Communications,* 2016, **7**, 10379.

31 D. Chen, F. Huang, Y. B. Cheng and R. A. Caruso, *Advanced Materials,* 2009, **2**, 2206–2210.

32 Z. Andaji-Garmaroudi and M. R. Mohammadi, *J. Am. Ceram. Soc.,* 2016, **99**, 167-173.

33 M. R. Mohammadi, Method for Preparing Titania Pastes for Use in Dye-Sensitized Solar Cells. U.S. Patent 8,906,711, 2014.

34 S. Mugundan, G. Rajamannan, N. Viruthagiri, R. Shanmugam and P. Gobi, *Appl. Nanosci.,* 2015, **5**, 449–456.

35 N. Hirata, J. J. Lagref, E. J. Palomares, J. R. Durrant, M. K. Nazeeruddin, M. Gratzel and D. Di Censo, *Chem. Eur. J.,* 2004, **10**, 595–602.

36 J. Gong, J. Liang and K. Sumathy, *Renew. Sust. Energ. Rev.,* 2012, **16**, 5848–5860.

37 L. Wei, P. Wang, Y. Yang, R. Fan, Y. Yang and Y. Qiu, *Sustainable Energy Fuels*, 2017, **1**, 1112-1122.